Analysis of flame acceleration in open or vented obstructed pipes

Vitaly Bychkov, Jad Sadek, and V'yacheslav Akkerman

Phys. Rev. E **95**, 013111 — Published 20 January 2017

DOI: 10.1103/PhysRevE.95.013111

Analysis of Flame Acceleration in Open/Vented Obstructed Pipes

Vitaly Bychkov[1,+] , Jad Sadek[2] and V'yacheslav Akkerman[2,*]

[1]*Department of Physics, Umeå University, Umeå 90187, Sweden* [+]Deceased

[2]*Center for Alternative Fuels, Engines and Emissions* (CAFEE)
Center for Innovation in Gas Research and Utilization (CIGRU)
Department of Mechanical and Aerospace Engineering, West Virginia University
Morgantown, WV 26506-6106, USA

Abstract

While flame propagation through obstacles is often associated with turbulence and/or shocks, Bychkov *et al.* [*Physical Review Letters 101 (2008) 164501*] have revealed a shockless, conceptually-laminar mechanism of extremely fast flame acceleration in semi-open pipes (one end of a pipe is closed; a flame is ignited at the closed end and propagates towards the open one). The acceleration is devoted to a powerful jet-flow produced by delayed combustion in the spaces between the obstacles, with turbulence playing only a supplementary role in this process. In the present work, this formulation is extended to pipes with both ends open in order to describe the recent experiments and modelling by Yanez *et al.* [*http://arxiv.org/abs/1208.6453*] as well as the simulations by Middha & Hansen [*Process Safety Progress 27 (2008) 192*]. It is demonstrated that flames accelerate strongly in open/vented obstructed pipes, and the acceleration mechanism is similar to that in semi-open ones (shockless, laminar), although acceleration is weaker in open pipes. Starting with an inviscid approximation, we subsequently incorporate hydraulic resistance (viscous forces) into the analysis for the sake of comparing its role to that of a jet-flow driving acceleration. It is shown that hydraulic resistance is actually not required to drive flame acceleration. In contrast, this is a supplementary effect, which moderates acceleration. On the other hand, viscous forces are nevertheless an important effect because they are responsible for the initial delay occurring before the flame acceleration onset, which was observed in the experiments and simulations. Accounting for this effect provides good agreement between the experiments, modelling and the present theory.

Keywords: open/vented obstructed pipes; hydraulic resistance; flame-flow interaction; flame acceleration; deflagration-to-detonation transition

*Corresponding Author:
V. Akkerman
Department of Mechanical and Aerospace Engineering
West Virginia University,
Morgantown, WV 26506-6206, USA
Phone: (+1) 304-293-0802 E-mail: Vyacheslav.Akkerman@mail.wvu.edu

I. Introduction

One of the critical fire safety demands is the prevention/mitigation of flame acceleration and deflagration-to-detonation transition (DDT). At the same time, the promotion of these processes is expected to improve advanced combustion technologies such as pulse-detonation and rotation-detonation engines as well as micro-combustors. Among the geometries associated with flame acceleration [1, 2] and DDT [3-5], obstructed pipes, presumably, provide the fastest regime of burning. While flame propagation through obstacles is often associated with turbulence [6] or shocks [7], a shockless, laminar and inviscid mechanism of extremely fast acceleration has been found for flame spreading through a "tooth-brush" array of obstacles in a "semi-open" pipe [8-10]. In such a configuration, one end of a pipe is closed such that a flame is ignited at the closed end, and it propagates towards the open one. This acceleration mechanism is devoted to a powerful jet-flow along the pipe centerline, generated by a cumulative effect of delayed burning in "pockets" between the obstacles, as detailed in *Sec. II*. This acceleration is extremely strong, and the mechanism is conceptually laminar, with turbulence playing only a supplementary role. To some extent, this makes the "tooth-brush" acceleration mechanism scale-invariant (Reynolds-independent) and, thereby, relevant to a variety of scales – from micro-combustors till industrial conduits as well as mining and subway tunnels.

However, while the studies [8-10] were limited to the semi-open channels and tubes, industrial and laboratory conduits often have both ends open, or vented, with a flame ignited at one of these ends. In particular, this is the case for the recent hydrogen-air experiments in vented obstructed conduits [11]. The experiments [11] have demonstrated strong flame acceleration, which would resemble that of Ref. [8], unless in the experiments, acceleration started not immediately after ignition, but following a noticeable delay, during which the flame propagated

almost steadily. Furthermore, while the formulation [8] is inviscid, the authors of Ref. [11] have devoted the entire acceleration scenario, observed in their experiments, to the viscous forces, following the studies [13, 14].

In addition to the experimental component, the study [11] also included ad-hoc numerical simulations performed by means of the combustion code COM3D. The simulations supported the experiments in that they also showed a delay prior to strong acceleration, and the locus of the transition to this accelerative regime was computationally prescribed quite well. However, the simulations overestimated the delay time. Such a discrepancy can be devoted to the chemical kinetics and other time-sensitive features from the practical reality that cannot be captured by the simulations. In addition, the FLACS simulations [12] also imitated the experiments [11], with better agreement on the delay time than that of the COM3D simulations. Still, the FLACS slightly underestimated of the locus of the acceleration onset.

Overall, the experiments [11] and the computational simulations [11, 12] identified a new phenomenon of near-steady flame propagation prior to a sudden transition to fast acceleration. In this respect, the major purpose of the present work is to elucidate and describe the experimental and computational findings [11, 12], in general, and the initial delay observed, in particular. For this purpose, the formulation [8] for semi-open obstructed channels is extended to that for open/vented ones (both ends of a channel are open). *First*, the inviscid approximation is kept, *Sec. III*, and it is shown that flame acceleration in the open obstructed pipes is qualitatively similar to that in the semi-open ones. Nevertheless, the acceleration rate in a pipe with both ends open is smaller because the flame-generated gas volume is distributed between the flows towards both open ends in this case, while in a semi-open pipe, the entire flow is pushed towards the single exit. *Second*, the viscous effects (hydraulic resistance) are incorporated into the analysis in

Sec. IV. As a result, good qualitative and quantitative agreement with the experiments [11] and the simulations [11, 12], including the initial delay prior to strong acceleration, is obtained. Specifically, it is found that the delay is related to hydraulic resistance, which opposes flame acceleration directly from the open pipe end.

As a result, in contrast to the statement of Ref. [11], devoting this acceleration to viscous effects, the present formulation shows that hydraulic resistance is not required at all to drive obstacles-based acceleration, which can be described even within the frame of an inviscid model. Nevertheless, the present study also justifies an important role of viscous forces: they hinder flame acceleration at the initial stages of combustion in obstructed conduits, thus causing a considerable delay in the onset of extremely strong acceleration.

II. Flame Acceleration in Semi-Open Obstructed Pipes

First, we briefly recall the physical mechanism of extremely fast flame acceleration in semi-open, obstructed channels, which has been identified in Ref. [8] and validated by numerical simulations [8, 9] and experiments [15]. Namely, we consider a two-dimensional (2D) channel of half-width R, with a part αR blocked by the obstacles in the form of a "tooth-brush" array of infinitely thin, parallel plates with spacing Δz between them; see Fig. 1. While we consider the obstacles to be placed close to each other with rather deep pockets, $\Delta z << \alpha R$, according to the computational simulations [9], the large spacing between the obstacles would not change the basic flame acceleration mechanism. Nevertheless, this might lead to noticeable complications of the analysis such as the need to account for the turbulent flow pulsations, which could actually conceal the main physical mechanism of flame acceleration. However, averaged-in-time, the turbulent pulsations would provide a minor (if any) contribution to the acceleration scenario [9].

The formulation [8] employed the conventional model of an infinitely thin flame front propagating locally with the laminar flame speed S_L. The initial stage of flame acceleration may be described in terms of an incompressible flow. Conceptually, the acceleration mechanism does not involve viscosity and turbulence; hence, it appears Reynolds-independent. A flame is ignited at the closed end, propagating fast towards the open end along the free part of the channel, and leaving the unburnt fuel mixture trapped in the pockets between the obstacles. The thermal expansion of the burning matter is characterized by the fuel-to-burnt density ratio, $\Theta \equiv \rho_f / \rho_b$, which is $3 \sim 8$ for typical fuels. Delayed burning in the pockets produces the extra gas volume, which flows out of the pockets with the velocity $(\Theta - 1)S_L$. The flow out of numerous pockets is deflected in the channel free part, and it is cumulated into a strong jet-flow along the channel axis, which drives the flame tip and produces new pockets. The positive feedback between the flame and the flow leads to powerful, extremely fast flame acceleration.

Due to the symmetry, only the upper half of the channel is considered, $x > 0$, with the *z*- and *x*-velocity components being $\mathbf{u} = (u; w)$. Delayed burning out of pockets sets the boundary condition in the burnt gas $w|_{x=(1-\alpha)R} = -(\Theta - 1)S_L$ for $z < Z_f$, where $Z_f(t)$ is the flame tip position. While the flame gets turbulized in the practical reality, according to Ref. [9], the curved (turbulent) shape of the flame tip provides a minor contribution into the acceleration mechanism and may be neglected. The solution to the incompressible continuity equation in the burnt gas, $\nabla \cdot \mathbf{u} = 0$, with the boundary condition at the closed channel end, $u|_{z=0} = 0$, yields the velocity distribution in the free part of the channel in the form

$$u = \frac{(\Theta - 1)S_L}{(1-\alpha)R} z, \qquad w = -\frac{(\Theta - 1)S_L}{(1-\alpha)R} x, \tag{1}$$

such that the flow velocity of the burnt gas at the flame tip position, $z = Z_f$, is

$$u(Z_f) = \frac{(\Theta - 1)S_L}{(1-\alpha)R} Z_f . \quad (2)$$

The flame tip velocity in the laboratory reference frame, $\dot{Z}_f$, is a sum of the flow velocity of the brunt gas, $u(Z_f)$, and the flame tip velocity with respect to the brunt gas, ΘS_L,

$$\frac{dZ_f}{dt} = \frac{(\Theta - 1)S_L}{(1-\alpha)R} Z_f + \Theta S_L . \quad (3)$$

Solution to Eq. (3), with the initial condition $Z_f(0) = 0$, takes the form

$$Z_f = \frac{\Theta R}{\sigma_s}\{\exp(\sigma_s S_L t / R) - 1\}, \quad (4)$$

with the scaled exponential acceleration rate

$$\sigma_s = \frac{\Theta - 1}{1-\alpha}, \quad (5)$$

where, the label "*s*" indicates a semi-open channel.

Equations (3) – (5) constitute the basics of the flame acceleration mechanism in semi-open channels with a "tooth-brush" set of the obstacles. This obstacles-based acceleration is very powerful, and it gets stronger with the increases in the blockage ratio α and the thermal expansion factor Θ. Say, for $\Theta = 8$ and $\alpha = 1/2$, Eq. (5) yields $\sigma_s = 14$. If a flame accelerated in the isobaric regime forever, this would imply the velocity increase by a factor of $\exp(14) \approx 10^7$ (!) during the characteristic burning time R/S_L. Obviously, such a huge velocity increase never happen in the practical reality because *(i)* the compressibility effects moderate flame acceleration at the developed stages [9, 10, 16] and *(ii)* a detonation would occur at much lower speeds. While obstacles-based acceleration resembles finger-shaped flame acceleration [16-18], the pockets filled with a fresh fuel mixture separate the free part of the channel from the walls enabling this acceleration to last longer than that of the finger flame model, where acceleration stops as soon as the flame front contacts the wall. In this light, to some extent, the tooth-brush mechanism can be treated as unlimited in time as long as the assumptions employed are justified.

III. Flame Acceleration in Open/Vented Obstructed Pipes: Inviscid Formulation

We next extend the analysis to a channel with both ends open and ignition occurring at the open end, as illustrated in Fig.2. Similar to *Sec. II*, here we still neglect the viscous effects; they will be accounted in *Sec. IV*. The conceptual difference between the semi-open and open pipes is that, in the latter configuration, the extra gas volume produced by delayed burning in the pockets is distributed at a certain turning point, Z_t, between two flows: *(i)* that of the burnt gas (label "1"), leaving the channel entrance, $z = 0$, with the velocity U_1; and *(ii)* that of the fuel mixture (label "2"), leaking through the channel exit, $z = L$, with the velocity U_2. Here L is the total length of the channel, but it is noted that the quantity L does not influence the formulation as long as viscosity is neglected.

The values U_1, U_2, Z_t are unknown *a priori* and have to be found from the momentum conservation. Specifically, we next assume a zero net force on the gas in the channel. Such an approach was successfully employed, in particular, in Ref. [19] for *unobstructed* pipes, where it allowed explaining a conceptual difference between flame acceleration in semi-open channels and quasi-steady flame propagation (oscillations) in open-open channels. It is nevertheless recognized that in the present, obstructed configuration a discontinuity along the line of the obstacles may create extra vortexes moving inside the gas flow and thereby influencing the net force. However, this effect is omitted in the present formulation and requires a separate study. Here, accounting for the balance of the momentum fluxes behind and ahead of the flame front, in the burnt matter and fuel mixture respectively,

$$P_b + \rho_b U_b^2 = P_f + \rho_f U_f^2 , \qquad (6)$$

with the relation $\Theta \equiv \rho_f / \rho_b$, and the pressure difference across the flame front, between the unburnt and burnt gases, in the form $P_f - P_b = (\Theta - 1)\rho_f S_L^2$, we find

$$U_b^2 = \Theta U_f^2 + \Theta(\Theta - 1)S_L^2 . \tag{7}$$

The quantities U_b and U_f generally may depend on time and tube length/position, so they may vary with the flame propagation. At the tube entrance and exit, they attain the values U_1 and U_2, respectively, such that Eq. (7) reads

$$U_1^2 = \Theta U_2^2 + \Theta(\Theta - 1)S_L^2 . \tag{8}$$

The matching condition at the flame front for the normal velocity component reads

$$U_2 - u(Z_f) = (\Theta - 1)S_L , \tag{9}$$

where $u(Z_f)$ is taken in the burnt gas just behind the flame front. Together, Eqs. (8) and (9) relates the velocities of the burnt gas at the entrance and just behind the flame, U_1 and $u(Z_f)$, as

$$U_1^2 = \Theta\left[u(Z_f) + (\Theta - 1)S_L\right]^2 + \Theta(\Theta - 1)S_L^2 . \tag{10}$$

Similar to *Sec. II*, we next solve the incompressible continuity equation, $\nabla \cdot \mathbf{u} = 0$, in the burnt gas but with the new boundary conditions for the *z*-velocity component,

$$u|_{z=Z_f} = u(Z_f), \qquad u|_{z=0} = -U_1, \qquad u|_{z=Z_t} = 0, \tag{11}$$

while the boundary conditions for *x*-velocity component are the same as in *Sec. II*. Then the counterpart of Eq. (1) becomes

$$u = \frac{(\Theta - 1)S_L}{(1-\alpha)R}(z - Z_t), \qquad w = -\frac{(\Theta - 1)S_L}{(1-\alpha)R}x . \tag{12}$$

Combining Eqs. (10) – (12), we find

$$u(Z_f) = \frac{(\Theta - 1)S_L}{(1-\alpha)R}(Z_f - Z_t), \tag{13}$$

$$\sqrt{\Theta\left[u(Z_f)+(\Theta-1)S_L\right]^2+\Theta(\Theta-1)S_L^2}=-u|_{z=0}=$$

$$\frac{(\Theta-1)S_L}{(1-\alpha)R}Z_t=\frac{(\Theta-1)S_L}{(1-\alpha)R}Z_f-u(Z_f). \qquad (14)$$

In the limit of strong flame acceleration, $u(Z_f)>>(\Theta-1)S_L$, $U_{1,2}>>(\Theta-1)S_L$, Eq. (10) reads $U_1\approx\sqrt{\Theta}U_2\approx\sqrt{\Theta}u(Z_f)$, and Eq. (14) is therefore reduced to

$$u(Z_f)=\frac{(\Theta-1)}{(1-\alpha)}\frac{Z_f}{\sqrt{\Theta}+1}\frac{S_L}{R}, \qquad Z_t=\frac{\sqrt{\Theta}Z_f}{\sqrt{\Theta}+1}. \qquad (15)$$

The transition from Eq. (14) to Eq. (15) is justified in Fig. 3, where both equations are solved and compared for the variety of expansion factors Θ and blockage ratios α. Specifically, the scaled flame tip position, Z_f/R, is plotted versus the scaled flow velocity at the front, $u(Z_f)/S_L$, for the fixed $\Theta=3.38$ (the same as in Ref. [11]) and various $\alpha=0.4,\ 0.5,\ 0.6$ in Fig. 3a; and for the fixed $\alpha=0.5$ and various $\Theta=3.38,5,8$ in Fig. 3b. It is seen that the difference between Eqs. (14) and (15) is minor for typical $\Theta=3\sim8$ and $1/3<\alpha<2/3$, which thereby justifies Eq. (15) that will be employed hereafter, and according to which $u(Z_f)$ in an open channel is $\sqrt{\Theta}+1$ times smaller than that in a semi-open one, Eq. (2). Also, the transition from Eq. (14) to Eq. (15), employing the approach $U_{1,2}>>(\Theta-1)S_L$, obviously allows neglecting the last term in Eq. (8) making it $U_1\approx\sqrt{\Theta}U_2$, or $U_1^2\approx\Theta U_2^2$. In this respect, the momentum fluxes balance equation, Eq. (6), written for the entire tube from the entrance to exit, splits into $\rho_b U_1^2=\rho_f U_2^2$ and $P_1=P_2=P_{amb}$. The latter equality simply denotes that the pressure at the open entrance and exit of the tube equals to the ambient (laboratory) pressure. Then the counterpart of Eq. (3) reads

$$\frac{dZ_f}{dt}=\frac{(\Theta-1)S_L}{(1-\alpha)R}\frac{Z_f}{\sqrt{\Theta}+1}+\Theta S_L, \qquad (16)$$

with the solution

$$Z_f = \frac{\Theta R}{\sigma_o}\{\exp(\sigma_o S_L t / R) - 1\}, \tag{17}$$

where

$$\sigma_o = \frac{\Theta - 1}{(\sqrt{\Theta} + 1)(1 - \alpha)} = \frac{\sigma_s}{\sqrt{\Theta} + 1} \tag{18}$$

is the scaled exponential acceleration rate and the label "*o*" stands for an open channel. Although the acceleration rate in an open channel, Eq. (18), is smaller than that in a semi-open one, Eq. (5), acceleration remains quite strong and, foremost, Reynolds-independent. To illustrate this statement, Fig. 4 presents a detailed parametric analysis of the present formulation and compares our results to the experimental data [11] as well as to the simulations [11, 12]. Specifically, Fig. 4a shows the time evolution of the flame tip position, $Z_f(t)$, Eq. (17), for the fixed $\Theta = 3.38$ and various $\alpha = 0.4 \sim 0.7$, while Fig. 4b presents $Z_f(t)$ versus time for the fixed $\alpha = 1/2$ and various $\Theta = 2.38 \sim 5.38$. The thermal expansion is essential for the burning time in the pockets, and therefore for the jet-flow towards to center of the channel. Indeed, according to Fig. 4a, the increase in Θ makes acceleration sudden, with no delay observed, while the reduction in Θ leads to a slight delay prior to strong acceleration. Nevertheless, this delay is still *far away* from that observed in Refs. [11, 12] as seen in Fig. 4c – the first attempt to compare the present study to the experimental and computational (COM3D) data [11] as well as to the FLACS simulations [12] for $\Theta = 3.38$, $\alpha = 1/2$, $R = 8.7\text{cm}$, and $S_L = 3.5\,\text{m/s}$. For these values, Eq. (18) yields $\sigma_o \approx 1.7$, implying a powerful acceleration: ≈ 5.5 times increase in the flame propagation velocity during a characteristic time $R/S_L \approx 0.025\text{sec}$. It is seen that both sets of simulations basically supported the experiments in terms of the acceleration rate and the general trend. In particular, they also identified a delay prior to strong acceleration (though the COM3D [11] overestimated the delay time by about 80% and its locus by almost 30%; while the FLACS [12]

overestimated the delay time by 20% and underestimated its locus by circa 30%). In contrast, all experimental and computational results [11, 12] disagree with the theoretical prediction of Eq. (17). Indeed, while the theoretical instantaneous acceleration rates of Fig. 4c can actually be compared to that of Refs. [11, 12], the delay observed in the experiments [11] and modelling [11, 12] cannot be predicted within an inviscid approach; it will be explained in *Sec. IV*.

IV. Flame Acceleration in Open/Vented Obstructed Pipes: Viscous Formulation

After ignition at the open end of the conduit and prior to sudden acceleration, the experiments [11] demonstrated almost steady, quasi-isobaric flame propagation with the speed $S_L \approx 3.5 m/s$, which lasts 1-2 sec, during which the flame overcomes 3-7 m, i.e. ½ - ¼ of the entire conduit. The COM3D [11] and FLACS [12] simulations have supported this result. The main purpose of this section is to find out the reason for such a delay by extending the formulation of *Sec. III* to account for viscous forces. It is natural to assume that viscosity influences the small scales first such that a flame front spreads as a "brush", and the upcoming formulation is devoted the dynamics of such a brush. It will be demonstrated below that the viscous effects in the brush modify the acceleration exponent, making it a time-dependent quantity. The sketches of the problem are shown in Fig. 5, which are more realistic than Fig. 2. Specifically, Fig. 5a presents an approximate schematic that will be employed in the formulation below, while the sketch in Fig. 5b is closer to the practical reality. Nevertheless, a flame front inside a pocket between the obstacles may actually be corrugated depending on a way how flame originally enters the pocket.

Since a flame may propagate rather slowly at the initial stages of the process, now we have to account for the finite length of the delayed burning zone. Namely, Z_b stands for the position of the last burning pocket in Fig. 5a. In the case of quasi-steady flame propagation, this position lags only slightly behind the flame tip, such that $Z_f - Z_b \approx \alpha R$ (here we approximate

that the flame in the pockets propagates with the laminar flame speed S_L and, hence, the time interval $\Delta t = \alpha R / S_L$ is required to burn one pocket). However, in the case of considerable flame acceleration, the lag may be quite large,

$$Z_f - Z_b \approx \frac{R}{\sigma_o} \exp(\sigma_o S_L t / R)\left[1 - \exp(-\alpha\sigma_o)\right]. \tag{19}$$

Substituting Eq. (17) into Eq. (19) yields

$$Z_f - Z_b \approx \left[Z_f + \frac{R}{\sigma_o}\right]\left[1 - \exp(-\alpha\sigma_o)\right]. \tag{20}$$

It is noted that Eq. (20) is valid for both strong and weak acceleration, yielding $Z_f - Z_b \approx \alpha R$ for $\sigma_o \to 0$. In the latter case, we should also account for the extra gas volume produced by the combustion process at the flame front in the free part of the channel, so the total flame-generated volumetric flow rate is

$$\frac{dV}{dt} = (\Theta - 1) S_L \left[Z_f - Z_b + (1 - \alpha) R\right] L_y, \tag{21}$$

where L_y is the channel width in the *y*-direction (perpendicular to the plane of Fig. 5a).

We next analyze the viscous forces produced by an accelerating flame front. Generally speaking, three viscous flows have to be considered: two flows to the right, $u > 0$, i.e. (*i*) that in the fuel mixture $(z > Z_f)$ and (*ii*) that in the burnt matter $(Z_t < z < Z_f)$; and (*iii*) one flow to the left, in the burnt matter, $u < 0$, $z < Z_t$. Nevertheless, being interested herein only in the initial stage of flame propagation (namely, in the delay prior to the acceleration onset), we approximate $Z_b \approx Z_t \approx Z_f$, having thereby only two viscous flows: for $z > Z_f$ and $z < Z_f$, respectively. Both the flows in the fuel mixture and the burnt matter are assumed to be plane-parallel shear flows, $u = u(x,t)$, of the same dynamic viscosity, $\eta = \rho\nu$, for which the Navier-Stokes equation reads [2]

$$\frac{\partial u}{\partial t} = -\Pi(t) + \nu \frac{\partial^2 u}{\partial x^2}, \tag{22}$$

with the boundary condition $u|_{x=(1-\alpha)R} = 0$, and $\Pi(t) = \rho^{-1} dP/dz$ being the scaled pressure gradient along the channel axis, which depends only on time in a shear flow. In a flow driven by exponential flame acceleration, we have $u \propto \Pi \propto \exp(\sigma S_L t / R)$, and Eq. (22) reduces to

$$\frac{\sigma S_L}{R\nu} u = -C_\Pi + \frac{d^2 u}{dx^2}, \tag{23}$$

where C_Π is a constant related to the pressure gradient. Solving Eq. (23) with the non-slip boundary conditions, $u = 0$ at $x = (1-\alpha)R$, we find (see Ref. [2] for the details of the method)

$$u(x,t) = \pm \frac{U_{1,2}(t)}{\cosh \mu_{1,2} - 1} \left[\cosh \mu_{1,2} - \cosh\left(\frac{\mu_{1,2} x}{(1-\alpha)R} \right) \right], \tag{24}$$

where $U_{1,2}(t) \propto \exp(\sigma S_L t / R)$ denote the maximal unburnt and burnt flow velocities attained at the channel axis, $x = 0$, and $\mu_1 = (1-\alpha)\sqrt{\sigma \,\mathrm{Re}/\Theta}$, $\mu_2 = (1-\alpha)\sqrt{\sigma \,\mathrm{Re}}$, with $\mathrm{Re} = \rho_f S_L R / \eta$ oftentimes named the Reynolds number associated with flame propagation. Unlike typical flow Reynolds numbers, the quantity Re is not related to any actual flow. However, it is an important descriptor of the flame dynamics. In particular, Re couples the radius of the channel with the size of the burning zone. Indeed, with the flame thickness defined, conventionally, as the ratio of the thermal diffusivity coefficient and the laminar flame speed, $L_f = D_{th} / S_L$, we obtain $\mathrm{Re} = \rho_f S_L R / \eta = S_L R / \nu = R / L_f \,\mathrm{Pr}$, where Pr is the Prandtl number. In the present theory, it is Re that describes the effect of viscosity as will be shown below. In the case of the experiments [11], the flame propagation Reynolds number was as large as $\mathrm{Re} \approx 2.02 \times 10^4$. With Eq. (24), the total volumetric flow rates are

$$\left(\frac{dV}{dt}\right)_{1,2} = L_y \int_0^{(1-\alpha)R} u\,dx = L_y \exp(\sigma S_L t/R)(1-\alpha)RU_{1,2}\frac{\cosh\mu_{1,2} - \mu_{1,2}^{-1}\sinh\mu_{1,2}}{\cosh\mu_{1,2} - 1}, \qquad (25)$$

and the continuity condition for the flows of the fuel mixture and the burnt matter yields

$$(\Theta - 1)S_L\left[\frac{Z_f - Z_b}{(1-\alpha)R} + 1\right] = U_1\frac{\cosh\mu_1 - \mu_1^{-1}\sinh\mu_1}{\cosh\mu_1 - 1} + U_2\frac{\cosh\mu_2 - \mu_2^{-1}\sinh\mu_2}{\cosh\mu_2 - 1}. \qquad (26)$$

With Eq. (20), Eq. (26) can also be rewritten as

$$(\Theta - 1)S_L\left\{\frac{Z_f + R/\sigma}{(1-\alpha)R}\left[1 - \exp(-\alpha\sigma)\right] + 1\right\} =$$

$$U_1\frac{\cosh\mu_1 - \mu_1^{-1}\sinh\mu_1}{\cosh\mu_1 - 1} + U_2\frac{\cosh\mu_2 - \mu_2^{-1}\sinh\mu_2}{\cosh\mu_2 - 1}. \qquad (27)$$

Equation (27) couples the quantities $U_{1,2}$ and Z_f. One more relation between them comes from the momentum fluxes balance. To be rigorous, we would have to integrate the velocity profiles (24) over the channel free path cross-section. However, since these profiles are almost "Π"-shaped for the realistically large $\mu_{1,2}$ (see Ref. [2] for the details), we can employ the evaluation

$$\int_0^{(1-\alpha)R} u^2\,dx \approx U_{1,2}^2(1-\alpha)R. \qquad (28)$$

With Eq. (28), averaging an inviscid counterpart of Eq. (6) over the channel free path cross-section yields

$$\left[\frac{\rho_f}{\Theta}U_1^2 - (\Theta - 1)\rho_f S_L^2\right](1-\alpha)RL_y = \rho_f U_2^2(1-\alpha)RL_y. \qquad (29)$$

Inviscid Eq. (29) is subsequently updated to incorporate the viscous forces. The viscous stresses in the burnt (label "1") and unburnt (label "2") gases, at the level of obstacle edges, are

$$\zeta_{1,2} = \left|\eta\frac{du}{dx}\right|_{x=(1-\alpha)R} = \frac{\mu_{1,2}\sinh\mu_{1,2}}{\cosh\mu_{1,2} - 1}\frac{\eta U_{1,2}}{(1-\alpha)R}, \qquad (30)$$

with the respective viscous forces

$$F_1 = \frac{\mu_1 \sinh \mu_1}{\cosh \mu_1 - 1} \frac{\eta U_1}{(1-\alpha)R} \frac{Z_f}{(1-\alpha)R} L_y (1-\alpha) R, \tag{31}$$

$$F_2 = \frac{\mu_2 \sinh \mu_2}{\cosh \mu_2 - 1} \frac{\eta U_2}{(1-\alpha)R} \frac{L - Z_f}{(1-\alpha)R} L_y (1-\alpha) R. \tag{32}$$

It is recalled that L is the total length of the channel. Unlike *Secs. II and III*, here L appears a parameter of the formulation as soon as the viscous effects are considered. For instance, the experiments [11] employed $L = 12.2\,\mathrm{m}$. It is also noted that *L* comes to play in the combination with the dynamic viscosity η (or, say, the kinematic viscosity ν), which should be another key parameter of the formulation. Specifically, the viscous stresses of Eq. (30) are proportional to η, and the viscous forces of Eqs. (31) and (32) are proportional to the combinations ηZ_f and $\eta (L - Z_f)$, respectively, such that Eqs. (30) – (32) yield zeros if $\eta \to 0$. With Eqs. (30) – (32), the viscous counterpart of Eq. (29) becomes

$$\frac{U_1^2}{\Theta S_L^2} + \frac{\mu_1 \sinh \mu_1}{\cosh \mu_1 - 1} \frac{U_1 Z_f}{(1-\alpha)^2 \,\mathrm{Re}\, S_L R} = \frac{U_2^2}{S_L^2} + \Theta - 1 + \frac{\mu_2 \sinh \mu_2}{\cosh \mu_2 - 1} \frac{U_2 (L - Z_f)}{(1-\alpha)^2 \,\mathrm{Re}\, S_L R}. \tag{33}$$

Eventually, the evolution equation for the flame tip reads

$$\frac{dZ_f}{dt} \approx \frac{\sigma S_L}{R} \left\{ Z_f + \frac{R}{\sigma} \right\} = U_2 \left(Z_f, \mathrm{Re} \right) + S_L. \tag{34}$$

Altogether, Eqs. (27), (33), and (34) describe flame acceleration in open obstructed channels accounting for the viscous effects. It is recalled that viscosity is incorporated into these equations by means of the flame propagation Reynolds number $\mathrm{Re} = \rho_f S_L R / \eta$ such that $\mathrm{Re} \to \infty$ if $\eta \to 0$.

V. Results and Discussion

The system of equations (27), (33) and (34) has been solved numerically for the variety of parameters α, Θ, Re and L, namely, $\alpha = 0.4 \sim 0.7$, $\Theta = 2.38 \sim 5.38$, $\mathrm{Re} = (1 \sim 4) \times 10^4$, and

$L = 10.2 \sim 14.2\,\mathrm{m}$. It is emphasized that while the exponential acceleration rate σ was a constant in the inviscid model, Eq. (18), the viscous forces make σ varying with the flame spreading along the channel. This is illustrated in Fig. 6, where the acceleration rate is plotted versus the flame tip position, $\sigma = \sigma(Z_f)$. All the plots show that although the "viscous" σ is less than the inviscid limit (18), it grows with Z_f and thereby strongly promotes the acceleration trend. Similar to *Sec. III*, here σ also grows with α, Fig. 6a, and with Θ, Fig. 6b, because both quantities provide a positive impact on flame acceleration, making the pockets deeper and the flame-generated volumetric flow rate larger, respectively. In contrast, an increase in the total channel length L promotes viscous effects and thereby reduces σ, as shown in Fig. 6c (though the dependence is relatively weak). As for the effect of the flame propagation Reynolds number Re, the acceleration rate σ emerges earlier but also saturates faster with the increase in Re, Fig. 6d. When $\mathrm{Re} \to \infty$, the inviscid formulation will be reproduced, with the time of initial near-steady flame propagation diminishing to zero, and σ approaching a constant value.

Figures 7 (a-d) are the counterparts of Figs. 6 (a-d) for the time evolution of Z_f at vairous α, Θ, Re and L. It is seen that the increase in σ during the flame spreading in a channel eventually leads to very strong acceleration, after a certain delay associated with almost steady flame propagation. It is recalled that such a delay was observed in Refs. [11, 12], experimentally and computationally, it was not found in the inviscid model of *Sec. III*, but it is identified now within the viscous formulation of Sec. IV. *Consequently, the delay is clearly attributed to the viscous effects*. According to Fig. 7, the delay decreases with α, Fig. 7a, and with Θ, Fig. 7b, because both these quantities facilitate acceleration. In contrast, the delay is larger for longer channels, Fig. 7c. The situation with the flame propagation Reynolds number is

opposite: the delay is reduced with the increase in Re. The latter fits our expectations: indeed, with $\mathrm{Re}\to\infty$, viscosity disappears from the present formulation and therefore no delay is seen.

It is also noted that the delay is inherent to open channels, while it has been observed neither experimentally nor computationally nor analytically in semi-open ones. Such a difference can be explained as follows. In a semi-open channel, the entire flame-generated volume is pushed towards the only exit (i.e. into the fuel mixture); the effect is very strong and it dominates over the viscous forces. In contrast, in a channel with both ends open, the flame-generated gas volume is distributed between two outward flows (to both ends). Since the momenta of these opposing flows almost balance each other, the role of viscous forces becomes noticeable, and it actually constitutes the focus of the present study. A similar mechanism has also been discussed in Ref. [19] but for unobstructed channels and tubes.

Eventually, Fig. 8 is an update of Fig. 4c, where the inviscid (*Sec. III*) and viscous (*Sec. IV*) formulations as well as the experiments [11] and the simulations [11, 12] are compared altogether. Specifically, $Z_f(t)$ is plotted for $\Theta=3.38$, $\alpha=1/2$, $\mathrm{Re}=2.02\times10^4$, $R=8.7\mathrm{cm}$, $L=12.2\,\mathrm{m}$, and $S_L=3.5\,\mathrm{m/s}$ [11]. Unlike Eq. (17), the present viscous formulation shows very good qualitative and good quantitative agreement with the experiments (in fact, it is better than that of the simulations [11, 12]; especially the ad-hoc simulations [12]), thereby justifying the present formulation.

Finally, it is recognized that the present work is only a pilot theoretical study of flame acceleration in obstructed open pipes, with a number of effects left beyond the consideration. In particular, similar to the theory of Ref. [8] for semi-open channels, the present formulation is incompressible; therefore, both analyses are acceptable only at the initial, near-isobaric stage of flame acceleration. In fact, a slight deviation between the experimental and theoretical plots in

Fig. 8 may be devoted to the effect of compressibility, which is neglected in the present work. Nevertheless, the suitability of the approach [8] has been validated computationally [8, 9] and experimentally [15]. The method how to incorporate compressibility in the analysis is developed in Ref. [10], for the semi-open obstructed channels, and it will be extended to the present configuration of pipes with both ends open elsewhere. Besides, while our theory is laminar, the flows and flames in obstructed pipes are turbulent in the practical reality [15], which provides an additional corrugation and, thereby, acceleration of the flame front. However "tooth-brush" acceleration is so strong and prompt that turbulence may provide only a supplementary impact as compared to this effect [9]. Furthermore, the present theory is 2D, while the real open/vented conduits are three-dimensional (3D). In this respect, our next aim is to reproduce the present analysis for a cylindrical axisymmetric open obstructed tube instead of a 2D channel. Such a task will be performed in the foreseeable future provided that a counterpart of the formulation [8] for cylindrical semi-open obstructed tubes has already been developed [9].

VI. Conclusions

In order to elucidate the recent experiments [11] and simulations [11,12], in the present work, the analytical formulation of extremely strong flame acceleration in "tooth-brushed" obstructed pipes [8] has been extended from the geometry of a semi-open 2D channel to that with both ends open. It is shown that flame acceleration in the open obstructed channels is very strong and, mechanistically, it is quite similar to that in the semi-open channels [8]: it is also shockless and conceptually laminar. Still, the acceleration rate in open channels is smaller than that in semi-open ones, and it varies during flame propagation.

It is noted that a number of assumptions and simplifications have been employed in the course of the derivations of Secs. II – IV, such as

- obstacles in the form an array of identical infinitely thin, parallel plates;
- axial symmetry;
- conventional model of an infinitely thin flame front propagating locally with the laminar flame speed S_L (including planar flame propagation in the pockets with the speed S_L);
- initial stage of flame acceleration is described in terms of an incompressible flow;
- flame tip is locally planar;
- zero net force on the gas in the channel (yielding Eqs. (6) and (29));
- strong flame acceleration (yielding Eq. (15));
- $Z_b \approx Z_t \approx Z_f$ such that only two viscous flows are considered;
- plane-parallel shear flows in the fuel and burnt gases, of the same dynamics viscosity;
- evaluation (28) fir the "Π"-shaped velocity profiles.

All these assumptions have been discussed when adopted in the present formulaiton, and their relevance has been verified when possible.

We started with an inviscid model, *Sec. III*, and then incorporated the viscous forces (hydraulic resistance) into the analysis in *Sec. IV*. A conceptual deference between the inviscid and viscous approaches is demonstrated. Specifically, is it is shown that the initial delay prior to the strong flame acceleration is attributed to the viscous effects because it has not been found in the inviscid model of *Sec. III*, but it has been identified within the viscous formulation of *Sec. IV*.

While Ref. [11] devoted the entire acceleration scenario to hydraulic resistance, the present work opposes this idea: it is shown that hydraulic resistance is not required to drive the obstacles-based acceleration, which can be explained within an inviscid model. Nevertheless, our formulation justifies an important role of hydraulic resistance: it hinders flame acceleration at the

initial stages of combustion, thus causing a considerable delay in the acceleration onset observed in the experiments [11].

Acknowledgements

This paper is the last analytical formulation of Vitaly Bychkov, who unexpectedly passed away when this work was in progress. The authors thank Mike Kuznetsov for the experimental data of Ref. [11]. They are also grateful to Damir Valiev, Cosmin Dumitrescu and Patrick Browning for the fruitful discussions. The work at West Virginia University has been supported by the U.S. National Science Foundation (NSF) through Akkerman's CAREER Award #1554254.

References

1. J.D. Ott, E.S. Oran, J.D. Anderson, *AIAA Journal* **41**, 1391 (2003).

2. V. Bychkov, A. Petchenko, V. Akkerman, L.-E. Eriksson, *Phys. Rev*. E **72**, 046307 (2005).

3. L. Kagan, G. Sivashinsky, *Combust. Flame* **134**, 389 (2003).

4. E.S. Oran, V.N. Gamezo, *Combust. Flame* **148**, 4 (2007).

5. S.B. Dorofeev, *Proc. Combust. Inst.* **33**, 2161 (2011).

6. M. Kuznetsov, V. Alekseev, I. Matsukov, S. Dorofeev, *Shock Waves* **14**, 205 (2005).

7. V.N. Gamezo, T. Ogawa, E.S. Oran, *Combust. Flame* **155**, 302 (2008).

8. V. Bychkov, D. Valiev, L.-E. Eriksson, *Phys. Rev. Lett.* **101**, 164501 (2008).

9. D. Valiev, V. Bychkov, V. Akkerman, C.K. Law, L.-E. Eriksson, *Combust. Flame* **157**, 1012 (2010).

10. V. Bychkov, V. Akkerman, D. Valiev, C.K. Law, *Combust. Flame* **157**, 2008 (2010).

11. J. Yanez, M. Kuznetsov, V. Bykov, "*Sudden Acceleration of Flames in Open Channels Driven by Hydraulic Resistance*," http://arxiv.org/abs/1208.6453.

12. P. Middha, O. R. Hansen, *Proc. Saf. Prog.* **27**, 192 (2008).

13. I. Brailovsky, G. Sivashinsky, *Combust. Flame* **122**, 492 (2000).

14. I. Brailovsky, L. Kagan, G. Sivashinsky, *Phil. Trans. R. Soc. London* A **370**, 625 (2012).

15. C.T. Johansen, G. Ciccarelli, *Combust. Flame* **156**, 405 (2009).

16. D. Valiev, V. Akkerman, M. Kuznetsov, L.-E. Eriksson, C.K. Law, V. Bychkov, *Combust. Flame* **160**, 97 (2013).

17. C. Clanet, G. Searby, *Combust. Flame* **105**, 225 (1996).

18. V. Bychkov, V. Akkerman, G. Fru, A. Petchenko, L.-E, Eriksson, *Combust. Flame* **150**, 263 (2007).

19. V. Akkerman, C.K. Law, V. Bychkov, L.-E. Eriksson, Phys. Fluids **22**, 053606 (2010).

FIGURES

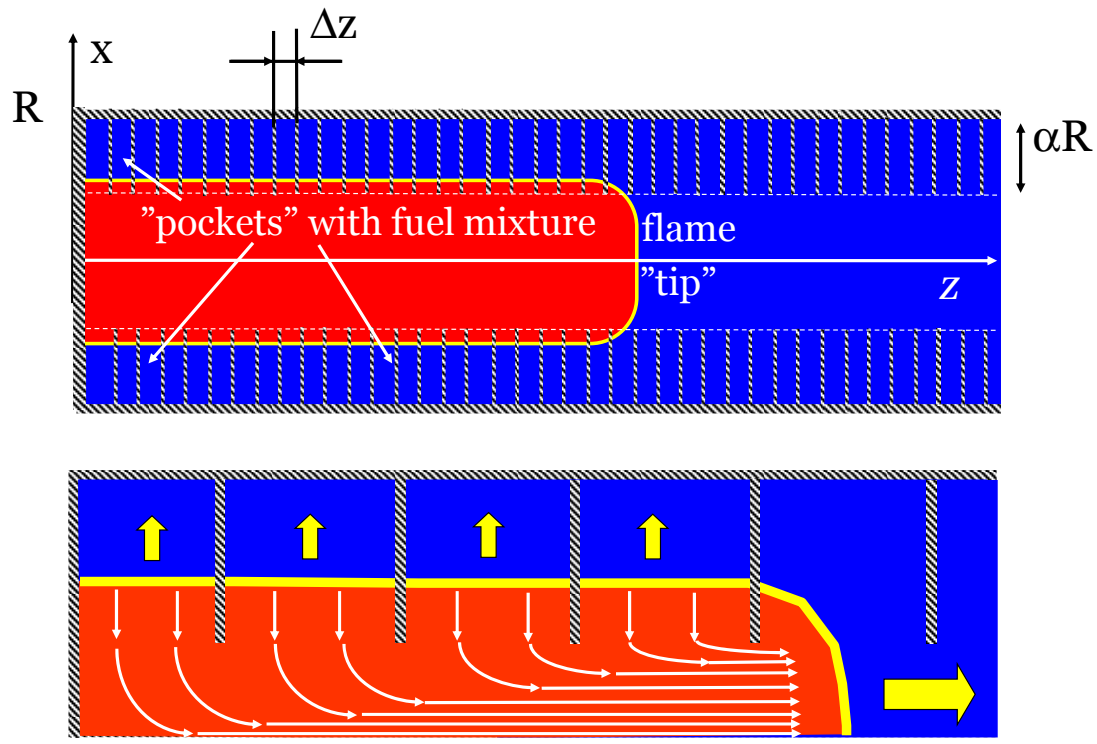

FIG 1: An illustration of *inviscid* flame propagation in a *semi-open* obstructed pipe.

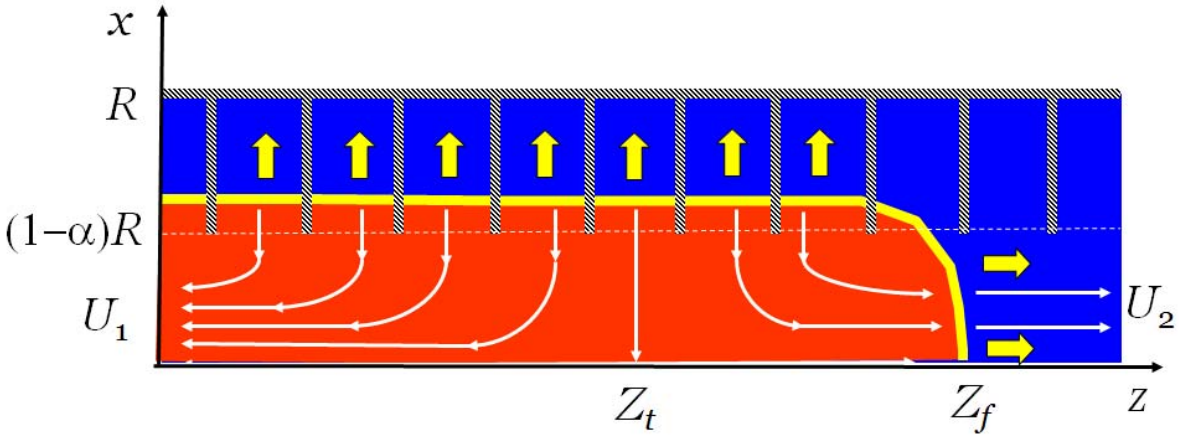

FIG. 2: An illustration of *inviscid* flame propagation in an *open* obstructed pipe.

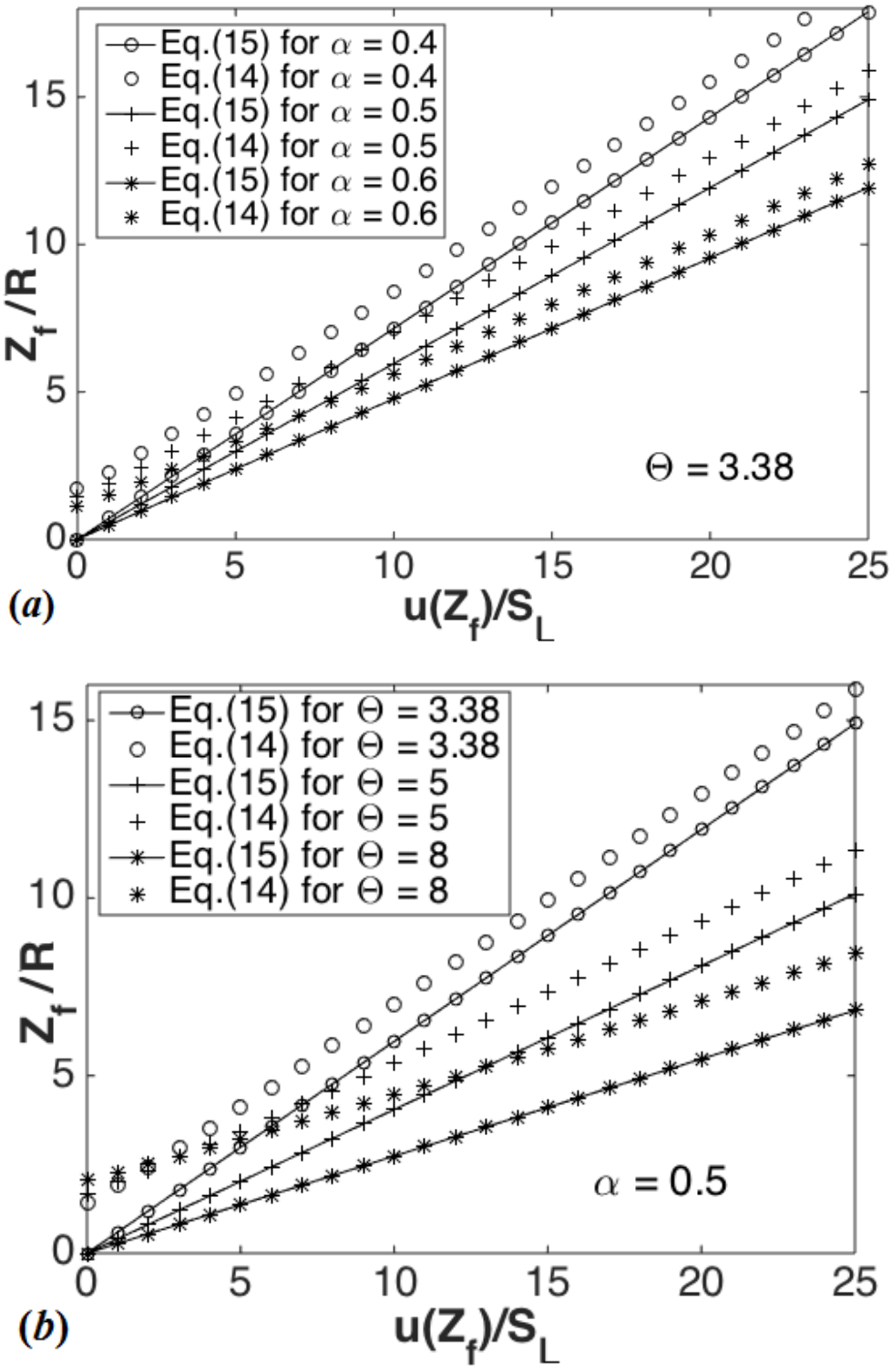

FIG. 3: Comparison of Eqs. (14) and (15): the scaled flame tip position, Z_f / R, versus the scaled flow velocity at the front, $u(Z_f)/S_L$, for various expansion factors Θ and blockage ratios α: a) $\Theta = 3.38$, $\alpha = 0.4, 0.5, 0.6$; b) $\alpha = 0.5$, $\Theta = 3.38, 5, 8$.

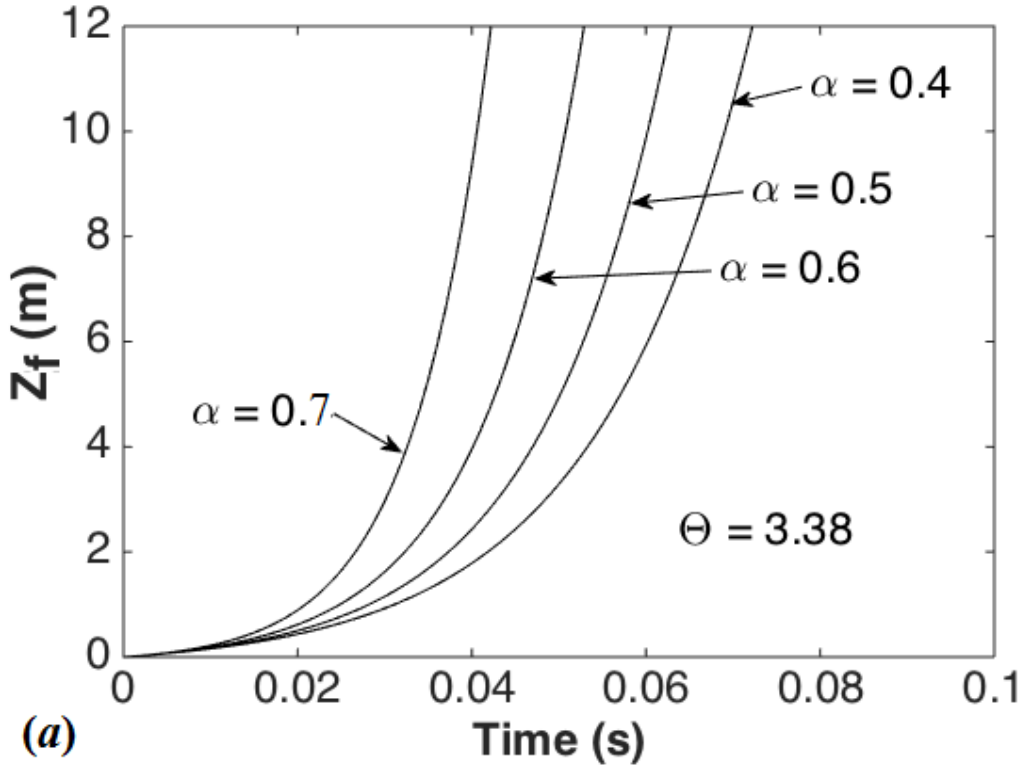
12
10
8
6
4
2
0
Z_f (m)
$\alpha = 0.4$
$\alpha = 0.5$
$\alpha = 0.6$
$\alpha = 0.7$
$\Theta = 3.38$
0
0.02
0.04
0.06
0.08
0.1
Time (s)

(a)

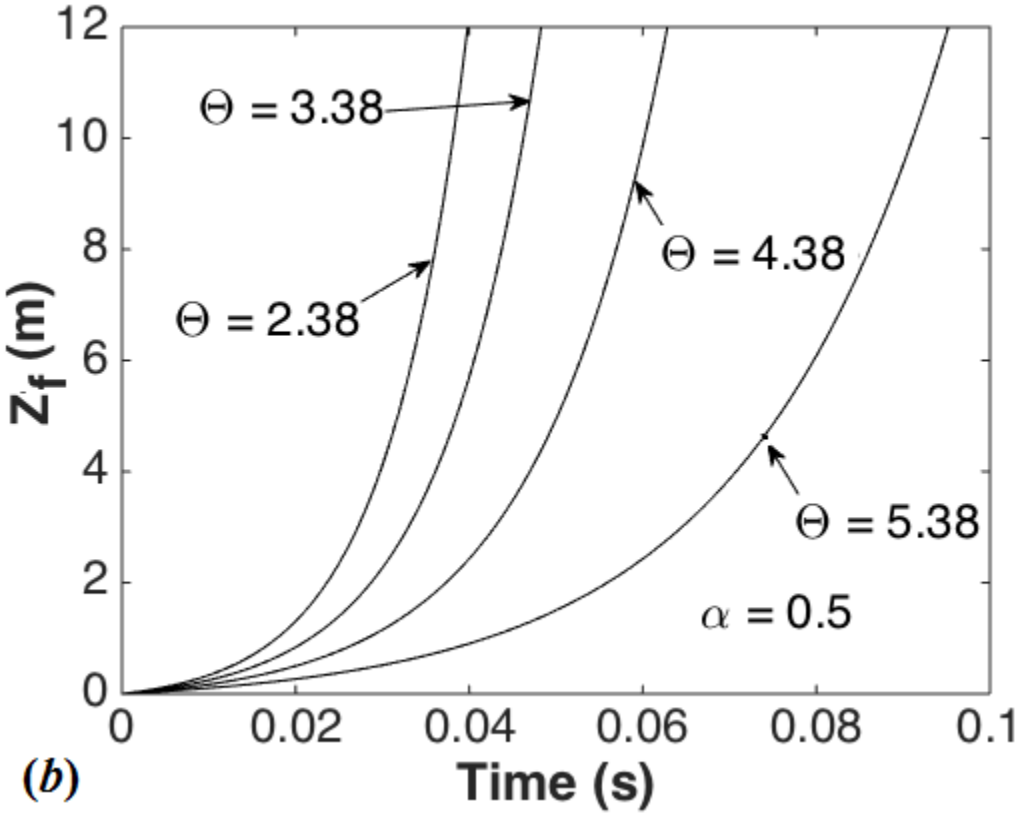
12
10
8
6
4
2
0
Z_f (m)
$\Theta = 3.38$
$\Theta = 2.38$
$\Theta = 4.38$
$\Theta = 5.38$
$\alpha = 0.5$
0
0.02
0.04
0.06
0.08
0.1
Time (s)

(b)

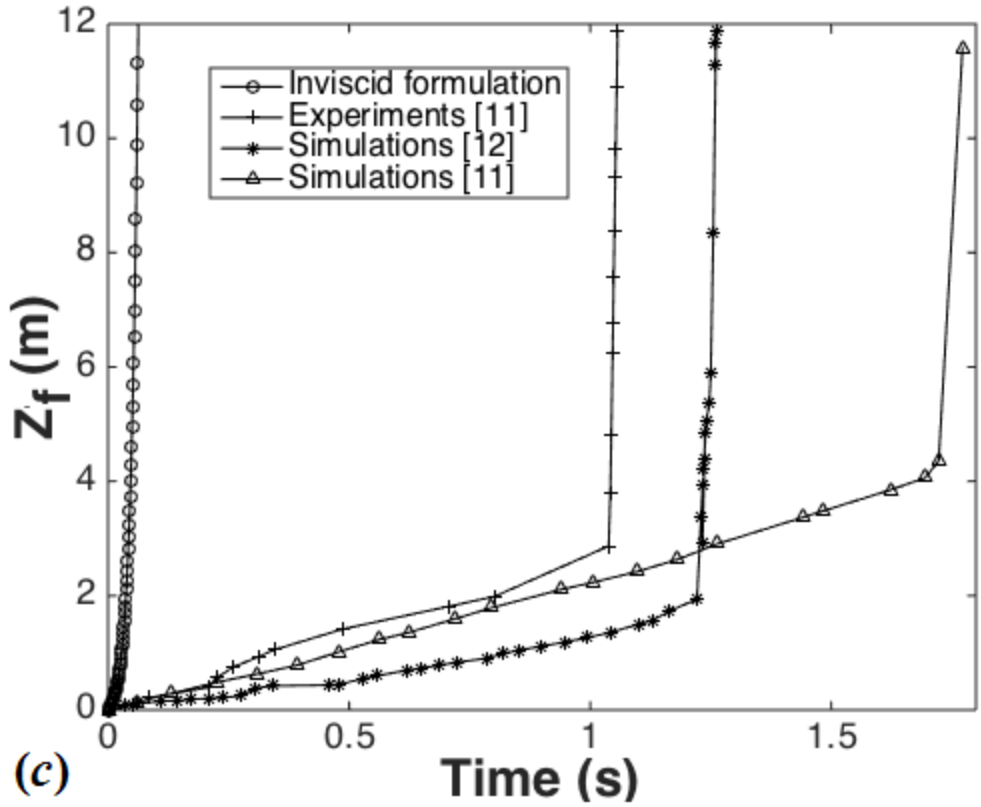

FIG. 4: Time evolution of the flame tip position, $Z_f(t)$, Eq. (17), for *a*) $\Theta = 3.38$, $\alpha = 0.4 \sim 0.7$; *b*) $\alpha = 1/2$, $\Theta = 2.38 \sim 5.38$; *c*) comparison to the experiments [11] and simulations [11, 12] for $\Theta = 3.38$, $\alpha = 1/2$, $R = 8.7\text{cm}$, and $S_L = 3.5\,\text{m/s}$.

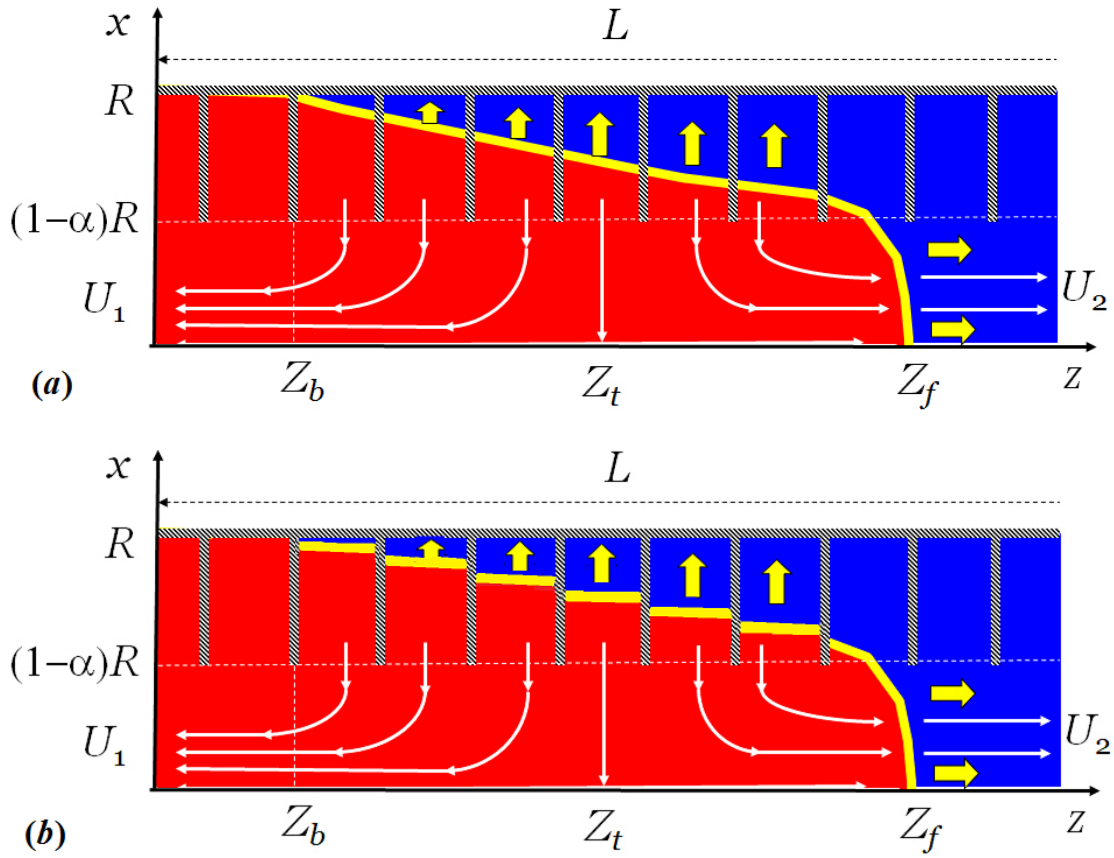

FIG. 5: Illustration of flame propagation in an open obstructed pipe (viscous formulation): the flame shape employed in the formulation (*a*) and a more realistic flame shape (*b*).

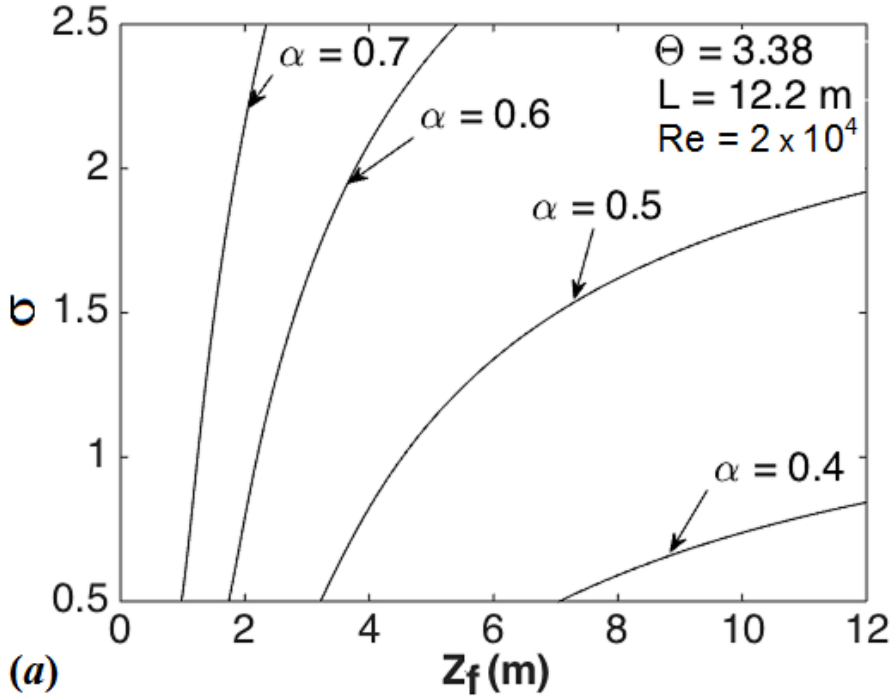
2.5
2
1.5
1
0.5
b
0
2
4
6
8
10
12
Z_f (m)
α = 0.7
α = 0.6
α = 0.5
α = 0.4
Θ = 3.38
L = 12.2 m
Re = 2 x 10^4

(*a*)

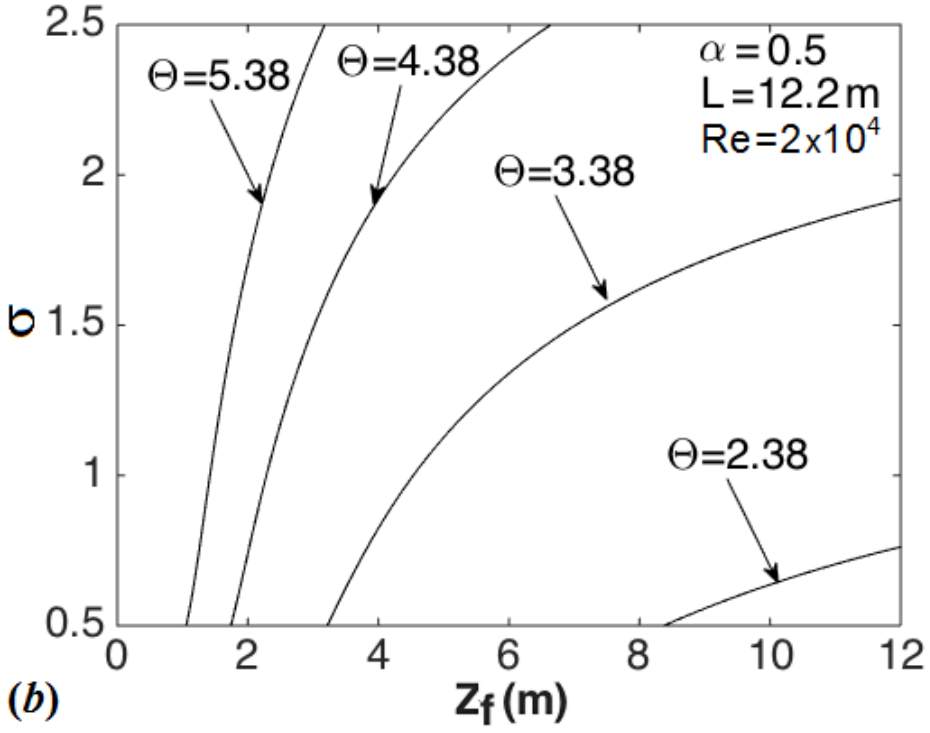
2.5
2
1.5
1
0.5
b
0
2
4
6
8
10
12
Z_f (m)
Θ=5.38
Θ=4.38
Θ=3.38
Θ=2.38
α = 0.5
L = 12.2 m
Re = 2x10^4

(*b*)

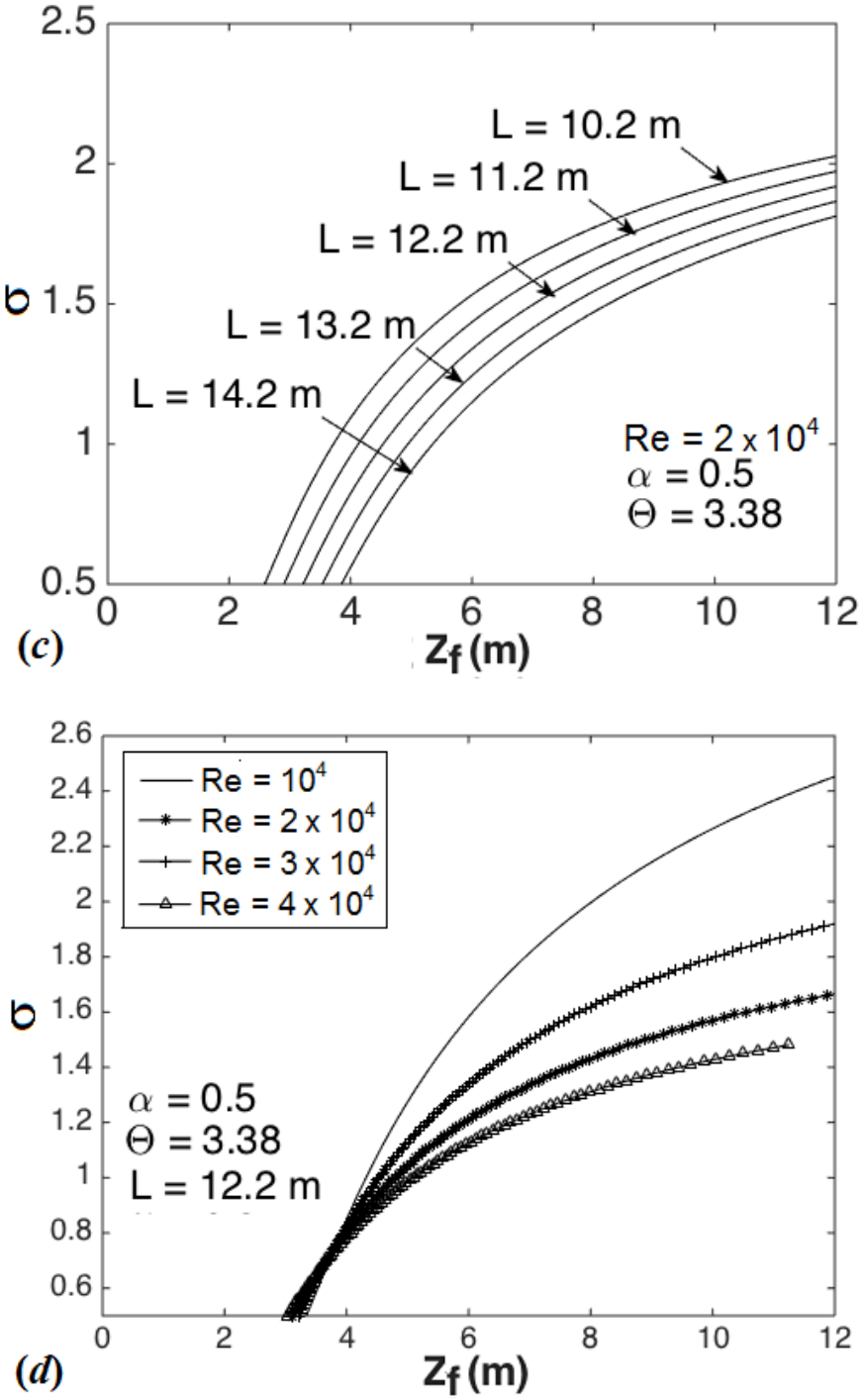

FIG. 6: Exponential acceleration rate σ versus the flame tip position Z_f for a) $\Theta = 3.38$, $L = 12.2\,\mathrm{m}$, $\mathrm{Re} = 2\times10^4$, $\alpha = 0.4 \sim 0.7$; b) $\alpha = 1/2$, $L = 12.2\,\mathrm{m}$, $\mathrm{Re} = 2\times10^4$, $\Theta = 2.38 \sim 5.38$ c) $\Theta = 3.38$, $\alpha = 1/2$, $\mathrm{Re} = 2\times10^4$, $L = (10.2 \sim 14.2)\,\mathrm{m}$; d) $\Theta = 3.38$, $\alpha = 1/2$, $L = 12.2\,\mathrm{m}$, $\mathrm{Re} = (1 \sim 4)\times10^4$.

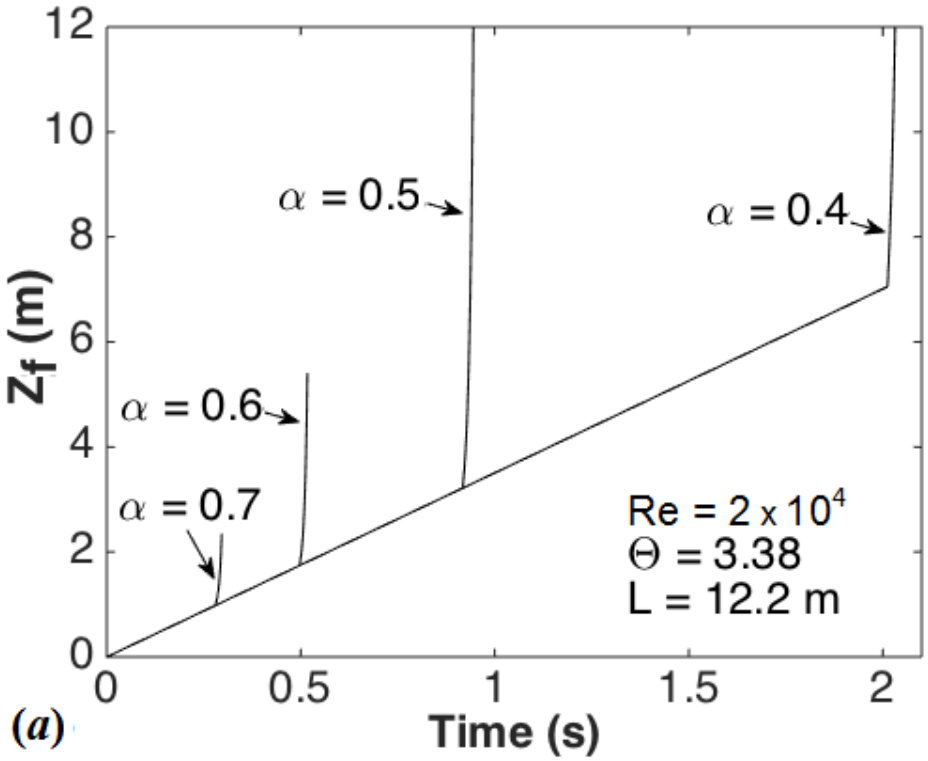
12
10
8
6
4
2
0
0
0.5
1
1.5
2
Zf (m)
Time (s)
α = 0.5
α = 0.4
α = 0.6
α = 0.7
Re = 2 x 10^4
Θ = 3.38
L = 12.2 m

(a)

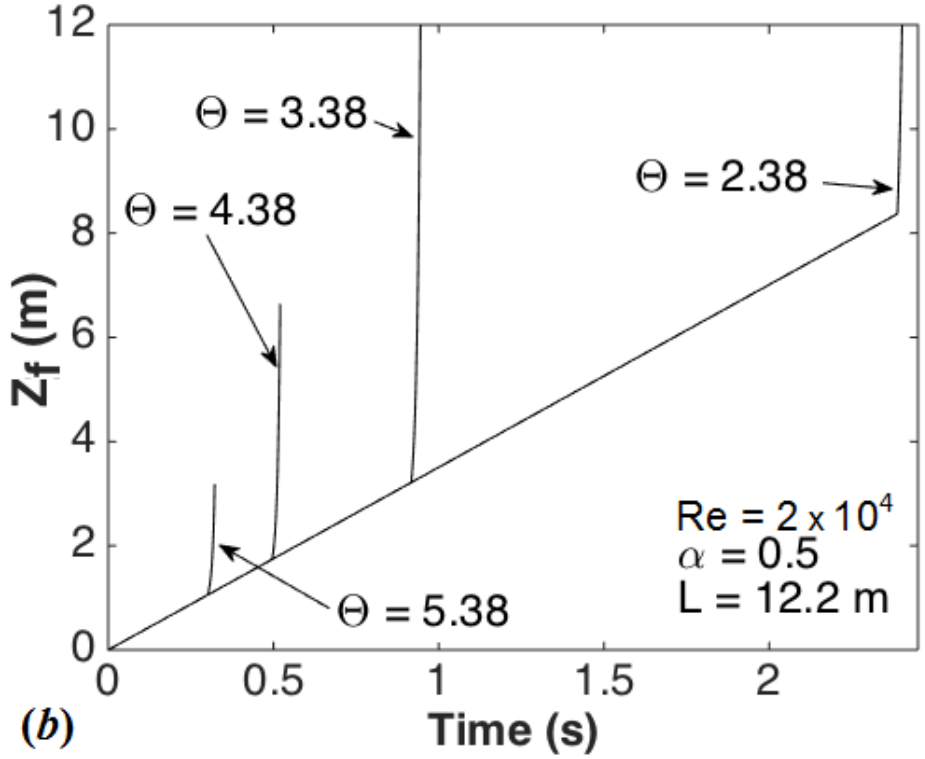
12
10
8
6
4
2
0
0
0.5
1
1.5
2
Zf (m)
Time (s)
Θ = 3.38
Θ = 2.38
Θ = 4.38
Θ = 5.38
Re = 2 x 10^4
α = 0.5
L = 12.2 m

(b)

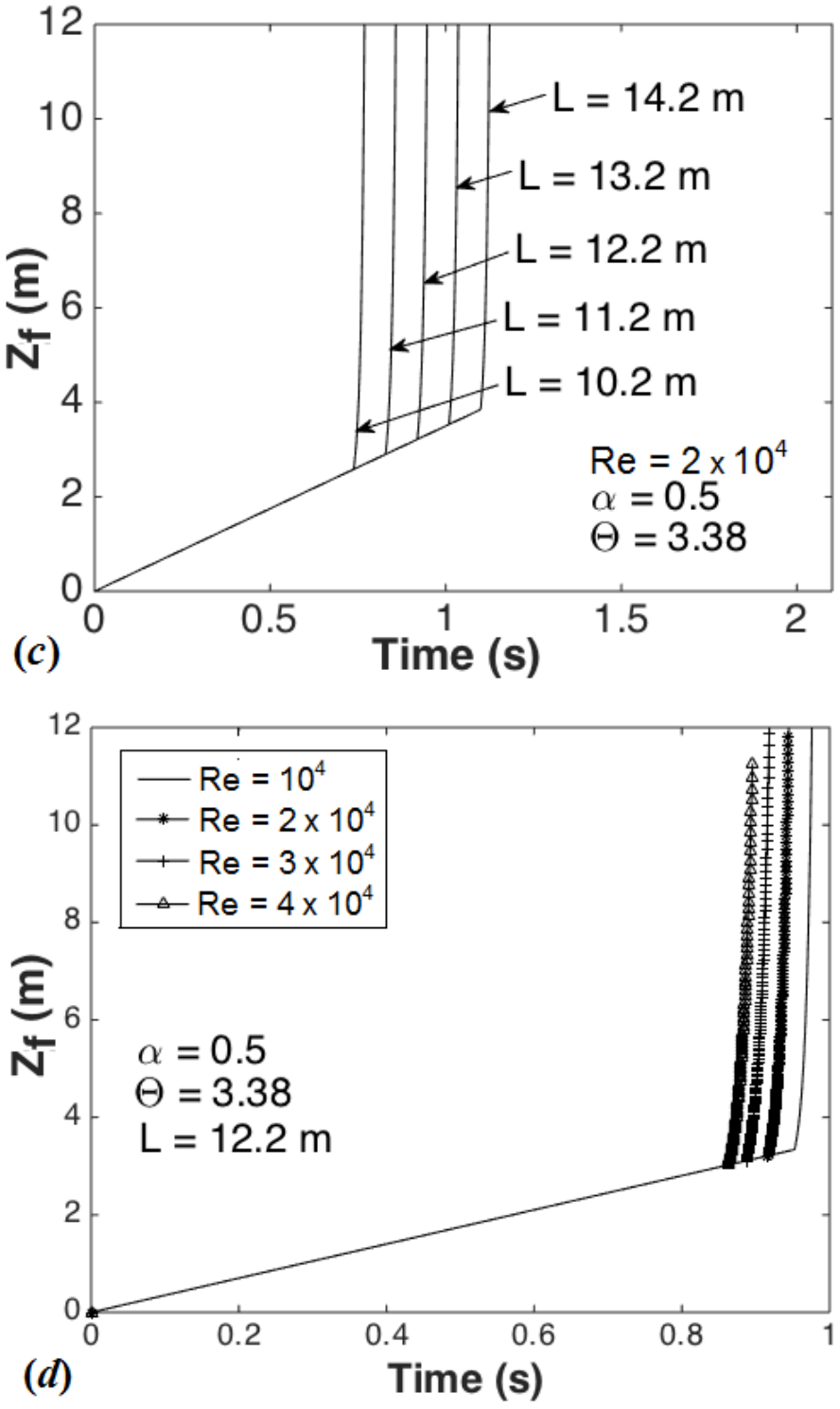

Fig. 7: Time evolution of the flame tip position, $Z_f(t)$ for a) $\Theta = 3.38$, $L = 12.2\,\mathrm{m}$, $\mathrm{Re} = 2\times10^4$, $\alpha = 0.4 \sim 0.7$; b) $\alpha = 1/2$, $L = 12.2\,\mathrm{m}$, $\mathrm{Re} = 2\times10^4$, $\Theta = 2.38 \sim 5.38$; c) $\Theta = 3.38$, $\alpha = 1/2$, $\mathrm{Re} = 2\times10^4$, $L = (10.2 \sim 14.2)\,\mathrm{m}$; and d) $\Theta = 3.38$, $\alpha = 1/2$, $L = 12.2\,\mathrm{m}$, $\mathrm{Re} = (1 \sim 4)\times10^4$.

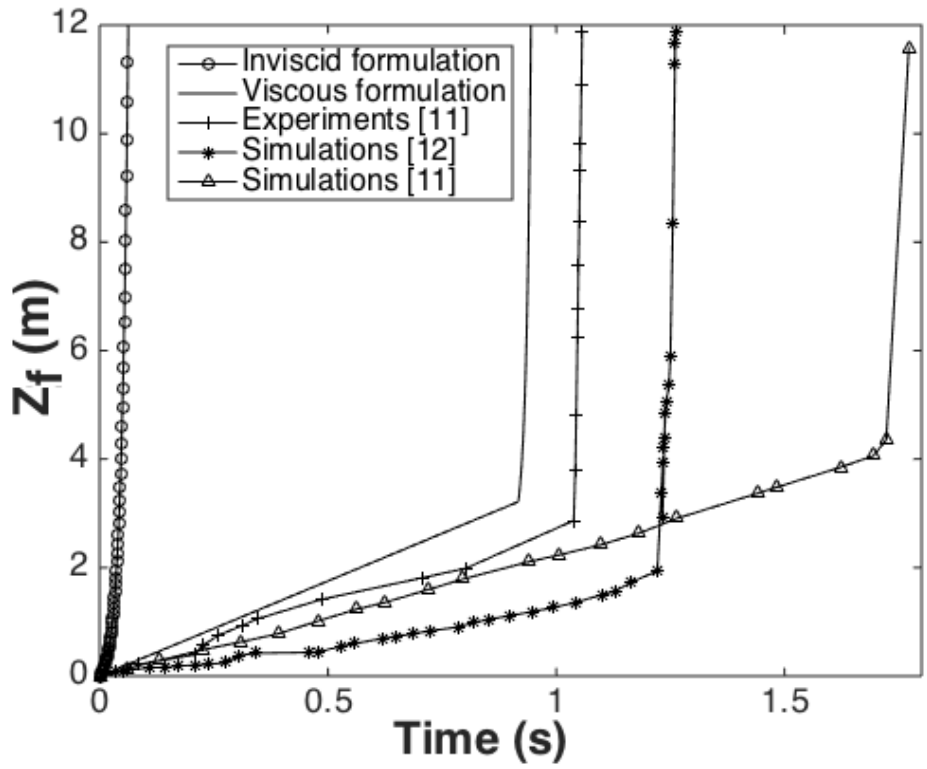

FIG. 8: Comparison of the inviscid and viscid formulations with the experiments [11] and the simulations [11, 12]: evolution of the flame tip position for $\Theta = 3.38$, $\alpha = 1/2$, $\mathrm{Re} = 2.02\times10^{4}$, $R = 8.7\mathrm{cm}$, $L = 12.2\,\mathrm{m}$, and $S_L = 3.5\,\mathrm{m/s}$.